Proceedings of the 2025 SICE Festival with Annual Conference
September 9-12, 2025, Chiang Mai, Thailand

Development of Small Binary Power Generator

Atsushi Koba[1†], Koichi Tsutsui[2], Kazuma Mera[3], Tomoki Usukura[4] and Hiroshi Kobayashi[5]

[1]Graduate School of Engineering, Tokyo University of Science, Japan
(Tel: +81-3-5876-1718; E-mail: a-koba@kobalab.com)
[2]Graduate School of Engineering, Tokyo University of Science, Japan
(Tel: +81-3-5876-1718; E-mail: tsutsu048@kobalab.com)
[3]Graduate School of Engineering, Tokyo University of Science, Japan
(Tel: +81-3-5876-1718; E-mail: kazuma.mera@kobalab.com)
[4]Graduate School of Engineering, Tokyo University of Science, Japan
(Tel: +81-3-5876-1718; E-mail: u.tomoki@kobalab.com)
[5]Graduate School of Engineering, Tokyo University of Science, Japan
(Tel: +81-3-5876-1718; E-mail: hiroshi@kobalab.com)

Abstract: There are a few cases in which medium- to low-temperature geothermal resources have been utilized for power generation. Therefore, we focused on binary power generation using hot spring water as a heat source. In this study, we developed a small binary power generator (10-15 kW) that can use medium- to low-temperature heat sources and confirmed its operation.

Keywords: Safety, Environment and Eco-Systems, Components and Devices

1. INTRODUCTION

Japan possesses the third-largest geothermal resources in the world (23.47 million kW), indicating significant potential for utilization. However, geothermal power currently accounts for only 0.3% of the country's total electricity generation. This is mainly because the dominant flash-type geothermal systems require high-temperature heat sources, and suitable sites for new development are limited [1]. Medium- to low-temperature heat sources (approximately 50–120 °C), which cannot be used in flash systems, are widely distributed across Japan but remain underutilized due to their dispersed and small-scale nature [2].

Against this background, small binary power generation systems utilizing medium- to low-temperature heat sources have been attracting increasing attention. The so-called "small" binary power systems typically produce electric power outputs ranging from several kilowatts to several hundred kilowatts, and primarily utilize heat sources in the temperature range of 70 to 130 °C. The following are representative classifications by output range and corresponding product examples in Japan.

- Less than 50 kW [3]-[5]: RHE 10kW system, HR series (HR20W), ECOR-3-Ft
- 50 kW–100 kW [6]-[7]: POWER + GENERATOR POWER+4400, MB-70H
- 100 kW–150 kW [8]-[10]: MB-125S, Thermapower 125MT, Mini-DTEC

In this way, although existing products are available in each output category, widespread adoption has been limited due to challenges such as maintenance costs caused by scale formation from hot spring water and restrictions on installation locations. For example, the device developed by Da Vinci Co. [3], which has an output of approximately 10 kW—comparable to the target output of this study—remains at the research stage and has not yet reached practical implementation.

In this study, we set a target of 10 kW, which is considered to be the minimum practical power generation capacity, and developed a small, portable binary power generation device with excellent maintainability and efficiency in this output range, where there are few existing products. The operation was experimentally verified, and the results are reported herein.

2. SYSTEM OVERVIEW

2.1 Power generation cycle

A schematic of the power generation system is shown in Fig. 1, and the external appearance in Fig. 2. The system operates on the Rankine cycle. The refrigerant (HFO-1233zd), pressurized by the refrigerant pump (Fig. 1(a)), is heated through heat exchange with hot water in the evaporator (b), turning into high-temperature vapor. This vapor rotates the rotor inside the rotary heat engine ((c), RHE, manufactured by Da Vinci), and is then condensed back into liquid in the condenser (d). The liquid refrigerant is stored in the refrigerant tank (e) and recirculated by the pump.

2.2 Engine output

The external appearance and internal flow paths of the RHE are shown in Fig. 3. The rotor in the RHE rotates due to the pressure difference between the inlet and outlet. The chamber volume is 1309 cc. Torque T [Nm] is given by Eq. (1), and power output W [W] is calculated using Eq. (2). The generator (Fig. 2(i)) is driven by connecting it to the RHE output shaft.

$$T\ [\mathrm{Nm}] = (\Delta P\ [\mathrm{kPa}] \times 1309\ [\mathrm{cc}] \times 10^{-3})/2\pi \quad (1)$$

$$W\ [\mathrm{W}] = 2\pi \times T\ [\mathrm{Nm}] \times N\ [\mathrm{rpm}]/60 \quad (2)$$

† Atsushi Koba is the presenter of this paper.

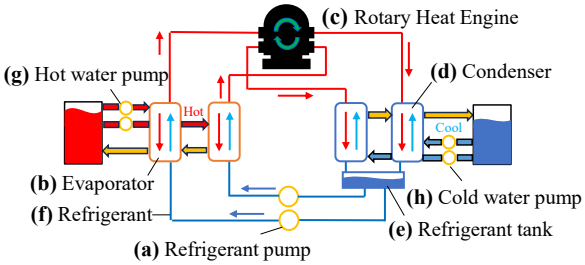

Fig. 1 System of binary power generator

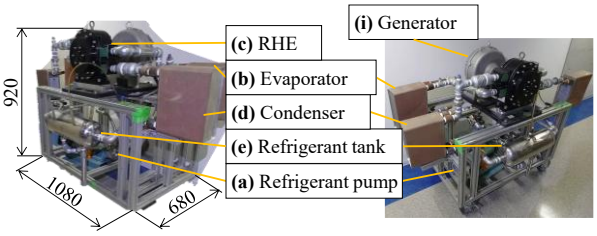

Fig. 2 External view

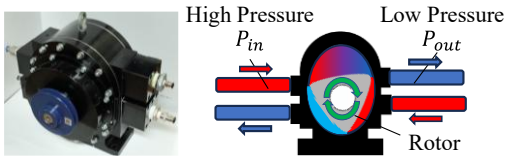

Fig. 3 Rotary heat engine

2.3 Constraints

As shown in Fig. 4, the binary power generation system involves numerous parameters, which are experimentally clarified in this study. (A) and (B) relate to refrigerant circulation. The refrigerant charge (A) is adjusted to ensure a constant liquid level in the refrigerant tank to prevent gas from entering the refrigerant pump. The height relationships between components (B) are determined by the piping layout. To prevent condensation and refrigerant stagnation inside the RHE, the piping from the evaporator to the RHE is inclined upward, and from the RHE to the condenser is inclined downward (i). The height arrangement between the refrigerant pump and the refrigerant tank (ii) ensures that the liquid level remains above the pump inlet by positioning the pump below the tank, stabilizing the discharge flow. (C) and (D) concern the rotation of the RHE. The arrangement of the evaporator (D) in parallel allows for an equal pressure to be applied to the two inlets of the RHE. The positioning of the condenser before the refrigerant tank (C) lowers the RHE outlet pressure because a stable liquid surface is formed when the refrigerant temperature is lower.

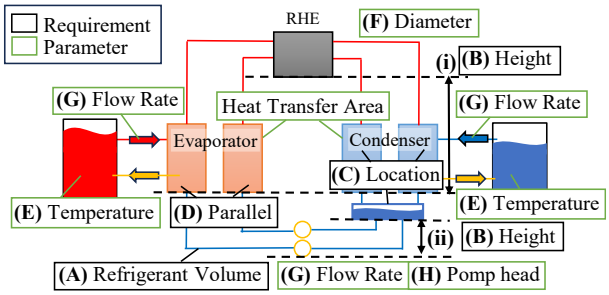

Fig. 4 Parameter of binary power generator

2.4 Selection of heat exchangers

In this study, commercially available plate heat exchangers were used for both the evaporator and the condenser, selected based on the following equations. The heat transfer amount Q [W] is calculated by Eq. (3), the required heat transfer area A [m²] by Eq. (4), and the logarithmic mean temperature difference ΔT_{im} by Eq. (5). Here, m represents the mass flow rate, C_p is the specific heat capacity of water at constant pressure, and U is the overall heat transfer coefficient; variables are defined by Eq. (6) and (7) as shown in Fig. 5.

$$Q = mC_p(T_{\mathrm{hw.in}} - T_{\mathrm{hw.out}}) \quad (3)$$

$$A = Q/U\Delta T_{im} \quad (4)$$

$$\Delta T_{im} = (\Delta T_i - \Delta T_i)/\ln(\Delta T_i/\Delta T_i) \ (i = 1,2) \quad (5)$$

$$\Delta T_{11} = T_{\mathrm{hw.out}} - T_{\mathrm{cR}} \quad (6)$$

$$\Delta T_{21} = T_{\mathrm{hw.in}} - T_{\mathrm{hR}} \quad (7)$$

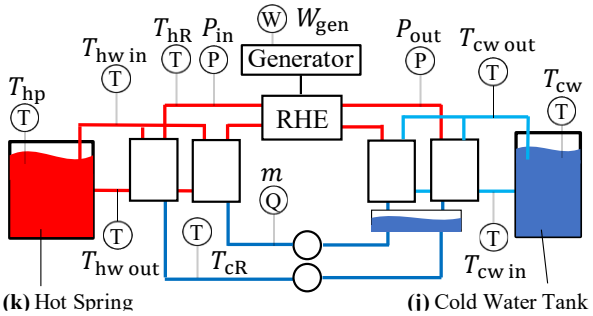

Fig. 5 Measuring points

3. SYSTEM IMPROVEMENTS

3.1 Parameter determination

The relationships of parameters (F) to (H) in Fig. 4 were experimentally identified, and their effects on system output were evaluated. The components used here were selected based on a target output of 2–3 kW.

3.2 Pipe diameter

The pipe diameter (F) affects the overall flow rate and pressure of the system. Components were connected using a combination of pipes ranging from 15A to 50A. Focusing on the areas around the RHE, which significantly influence output, six configurations were tested: evaporator to RHE inlet with 25A, 32A, and 40A pipes, and RHE outlet to condenser with 40A and 50A pipes. The results are shown in Table 1 and Fig. 6.

These results indicate that increasing the pipe diameter decreases the pressure at both the inlet and outlet of the RHE, but consequently increases power output. This is likely due to a reduction in pressure loss at the inlet, allowing a greater amount of vapor to enter the RHE. However, when the inlet and outlet pipe diameters of the RHE are the same, the output decreases, likely because no pressure difference is generated due to the uniform pipe diameter.

The pipe diameter from the refrigerant tank (e) to the refrigerant pump (a) was also changed to 15A and 25A, but no significant change in pump flow rate was observed, indicating that other components such as the evaporator and refrigerant pump have a greater impact. However, if

air accumulates in the piping, the flow rate drops sharply, requiring careful piping design.

Table 1 Pipe diameter

Condition			W_{RHE} [W]	P_{in} [MPa]	P_{out} [MPa]	ΔP [MPa]	N [rpm]
	In	Out					
1-1	25A	40A	188	0.24	0.19	0.05	300
1-2	32A		523	0.22	0.18	0.04	500
1-3	40A		462	0.19	0.15	0.04	470
1-4	25A	50A	423	0.19	0.16	0.03	450
1-5	32A		523	0.21	0.18	0.03	500
1-6	40A		633	0.20	0.15	0.06	550

3.3 Pump performance

The refrigerant pump affects the RHE pressure difference ΔP in Eq. (1) and the mass flow rate m in Eq. (3) according to flow rate (G) and head (H). Experiments were conducted using two pumps with heads of 4 m and 6 m, and the flow rate was varied using a valve. The results are shown in Table 2 and Fig. 7.

Although it was assumed in the Rankine cycle model that ΔP would increase by 0.01 MPa for every 1 m increase in pump head, it was observed that pressure increased not only with head but also with increased flow rate. This is because more refrigerant is vaporized in the evaporator, resulting in the compression of a larger volume of vapor.

Table 2 Pomp head and Flow rate

	Head [m]	Flow [L/min]	W_{RHE} [W]	P_{in} [MPa]	P_{out} [MPa]	ΔP [MPa]
2-1	4	7	482	0.215	0.19	0.025
2-2	6	9	753	0.225	0.18	0.045
2-3	6	13	1026	0.234	0.17	0.064

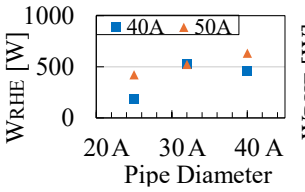

Fig. 6 Diameter and W_{RHE}

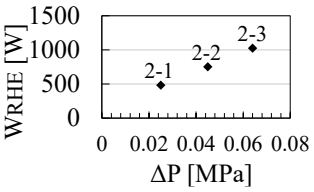

Fig. 7 ΔP and W_{RHE}

The flow rates of the hot and cold water pumps are determined based on the heat exchange amount in Eq. (3), depending on the balance between temperature conditions and refrigerant flow rate. The required pump head is determined by pressure losses in the heating unit as described later and the number of plates in the heat exchanger.

3.4 Heating units

Hot spring water contains dissolved minerals that can precipitate as solid scale, which may clog pipes or coat metal surfaces, reducing thermal efficiency. To avoid these issues, a heating unit is submerged in the hot spring and tap water, or groundwater is circulated through the unit to produce hot water, which then transfers heat to the refrigerant in the evaporator.

The required performance of the heating unit to achieve the target output of 10 kW, based on the Rankine cycle approach described later, is a hot water flow rate of 60 L/min and a hot water temperature $T_{hw.in}$ of 80 °C.

Three types of heating units were tested, as shown in Fig. 8 Unit (I) used steel pipes and fittings arranged in a grid structure. Unit (II) adopted a box shape to increase thermal capacity. However, both units failed to provide sufficient heat exchange and could not maintain the required hot water temperature. Therefore, Unit (III) employed copper pipes with high thermal conductivity, a diameter of 25 mm, and a total length of 30 m. Its performance was validated through field testing.

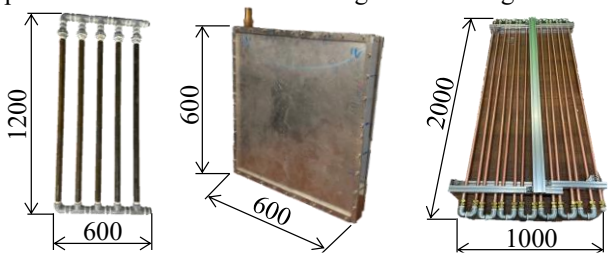

Fig. 8 Heating unit types

4. DEMONSTRATION TEST

4.1 Experimental method

An operational test of the developed small binary power generation system was conducted to verify whether the target output of 10 kW could be achieved. The test site and heat source were the Tamano-yu hot spring (Izu-Atagawa, natural outflow temperature 100 °C). The measured parameters, shown in Fig. 5, were RHE rotational speed N, RHE inlet and outlet pressures P_{in} and P_{out}, refrigerant temperatures T_{hR} and T_{cR}, hot water temperatures $T_{hw.in}$ and $T_{hw.out}$, refrigerant pump flow rate m_R, and hot water flow rate m_{hw}.

4.2 Experimental conditions

A Rankine cycle targeting 10 kW output was assumed on a p-h diagram, as shown in Fig. 9. The enthalpy values at each component were denoted as ($h1$) to ($h4$). Setting the RHE inlet conditions at a refrigerant temperature of 60 °C and pressure of 0.29 MPa, and the RHE outlet at a refrigerant temperature of 30 °C and pressure of 0.05 MPa, the RHE output was calculated as 11.3 kW at a flow rate of 30 L/min based on Eq. (8).

Based on this, components were selected: the refrigerant pump (a) was specified for a head of 30 m and flow rate of 30 L/min corresponding to a pressure difference of 0.24 MPa; the evaporator (b) and condenser (d) each had a heat transfer area of 2.8 m² with 100 plates; the hot water pump (g) had a head of 8.6 m and flow rate of 60 L/min; and the cold water pump (h) had a head of 8.6 m and flow rate of 60 L/min. Three experiments were conducted: motors with different outputs (1.5 kW and 30 kW) were connected to the generator (i) to vary the load, and the pipe diameter from the evaporator to the RHE was changed between 32A and 40A.

$$W_{RHE} = m_R \times (h_3 - h_4) \quad (8)$$

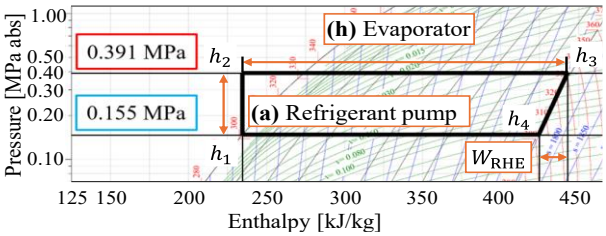

Fig. 9 Hypothetical pressure enthalpy chart

4.2 Experimental results

The measurement results are shown in Table 3, and the cycle under experimental condition 3-3 is illustrated in Fig. 10. The maximum generated power was 1.02 kW, and the RHE output was 3.83 kW. Additionally, Table 4 presents the performance of the heating unit, represented by the hot water temperature $T_{\mathrm{hw.in}}$ and the hot water pump flow rate m_{hw}.

Table 3 Experimental results

Condition			P_{in} [MPa]	P_{out} [MPa]	N [rpm]	W_{gen} [kW]
	Motor	φ D				
3-1	1.5 kW	32A	0.15	0.10	1865	0.07
3-2	30 kW	32A	0.34	0.12	679	1.01
3-3	30 kW	40A	0.28	0.11	1021	1.02

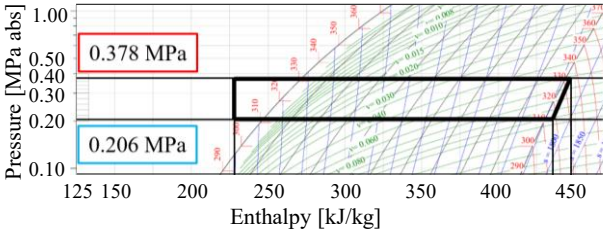

Fig. 10 Pressure enthalpy chart

Table 4 Performance of the heating unit

Condition	$T_{\mathrm{hw.in}}$ [℃]		m_{hw} [L/min]
	start	5min later	
3-1	80.2	78.3	30
3-2	82.1	77.5	30
3-3	80.0	76.7	30

4.4 Performance evaluation and discussion

In this test, the target output of 10 kW was not achieved.

The results of the following calculations are shown in Tables 5 to 7. Based on Table 3, the RHE rotational torque T, RHE output W_{RHE}, and heat exchange amount of the hot water Q_{hw} were calculated using Eqs. (1) to (3), the theoretical heat exchange amount of the hot water $Q_{\mathrm{hw\_th}}$ was calculated based on the enthalpy values obtained from Fig. 9, and the thermal efficiency η, calculated from Eq. (9).

$$\eta = W_{RHE} / Q_{\mathrm{hw}} \quad (9)$$

Table 5 shows the relationship between the load applied by the motor connected to the generator and the differential pressure applied to the RHE. These results indicate that an increase in load due to the motor connected to the generator results in greater work output W_{RHE} from the RHE. This is believed to be due to the increased compression of the vaporized refrigerant from the evaporator, which results in a higher differential pressure ΔP. However, since the load was too large, the refrigerant pump flow rate m_R decreased.

Similarly, significant piping losses in the heating unit resulted in a reduced flow rate. As shown in Table 6, the actual hot water pump flow rate was only 30 L/min compared to the expected 60 L/min, leading to insufficient heat exchange amount Q_{hw} with the refrigerant. Consequently, as illustrated in Table 2, the anticipated pressure increase due to the combined effects of pump head and vapor compression could not be achieved. Furthermore, as indicated in Table 4, the hot water temperature $T_{\mathrm{hw.in}}$ decreased within five minutes of the experiment's initiation, demonstrating inadequate heat exchange performance. Therefore, improvements are required both in reducing piping losses and enhancing the heat exchange performance.

On the other hand, as shown in Table 7, when the pipe diameter was increased, although the pressure decreased, in RHE output. This is likely because, as seen in Table 1, the increased pipe diameter allowed for smoother vapor flow, enabling enough vapor to enter the RHE relative to its volume, thereby improving thermal efficiency.

Table 8 presents a comparison between the thermal efficiency obtained from the demonstration experiment, $\eta_{exp.}$, and the theoretical maximum thermal efficiency of a heat engine, i.e., the Carnot efficiency η_{Carnot} (Eq. (10)), assuming a high-temperature source of T_{hot} = 80 ℃ and a low-temperature sink of T_{cold} = 30 ℃. The corresponding Carnot achievement ratio R_{Carnot} (Eq. (11)) is also included.

From these results, it is evident that Condition 3-3, in which the pipe diameter was increased, achieved the highest Carnot efficiency ratio. To further improve thermal efficiency, it will be necessary to minimize the pinch temperature between the refrigerant and the heat source/cooling water, improve pump efficiency, and identify and reduce pressure losses in the piping system, which are not yet sufficiently considered.

$$\eta_{Carnot} = 1 - T_{cold} / T_{hot} \quad (10)$$

$$R_{Carnot} = \eta_{exp.} / \eta_{Carnot} \quad (11)$$

From the above, it was found that the necessary improvements to achieve an RHE output of 10 kW include increasing the refrigerant pump flow rate from 22 L/min to 30 L/min, increasing the hot water pump flow rate from 30 L/min to 60 L/min, and optimizing the power generation load to obtain the optimal differential pressure. Concurrently, maintaining the hot water temperature at 80 °C is also required for stable operation. Furthermore, along with these improvements, there is a possibility of increased losses in each component and an imbalance in the heat balance between the evaporator and condenser sides; thus, it is necessary to improve thermal efficiency and adjust the overall energy balance of the system.

Table 5 Effect of power generation load on performance

Condition			ΔP [MPa]	T [Nm]	W_{RHE} [kW]
	Motor	φ D			
3-1	1.5 kW	32A	0.05	9.2	1.79
3-2	30 kW		0.22	45.0	3.20

Table 6 Evaluation of heating unit

Condition	m_{hw} [L/min]	Q_{hw} [kW]	$Q_{\mathrm{hw\ th}}$ [kW]
3-1	30	20.37	124.8
3-2		49.30	
3-3		31.78	

Table 7 Effect of pipe diameter on performance

Condition			P_{in} [MPa]	ΔP [MPa]	W_{RHE} [kW]	η [%]
	Motor	φ D				
3-2	30 kW	32A	0.34	0.22	3.20	6.49
3-3		40A	0.28	0.17	3.83	12.06

Table 8 Thermal efficiency comparison

Condition	$\eta_{exp.}$ [%]	η_{Carnot} [%]	R_{Carnot} [%]
3-1	8.79	14.16	62.1
3-2	6.49		45.8
3-3	12.08		85.3

5. CONCLUSION AND FUTURE WORK

In this study, a small binary power generation system was developed, and its performance was evaluated through field testing. Although the target output was not achieved, new insights were obtained. Based on these results, future work will involve systematically organizing the overall parameters and clarifying the interrelationships from three perspectives: (α) the design of the system itself, (β) the selection of generators and load settings, and (γ) the improvement of heat source utilization efficiency, such as optimizing the use of hot springs.

With these improvements, long-term operational tests will be conducted at a demonstration site following the achievement of 10 kW output, in order to evaluate the continuous operational performance and durability of the system components. In addition, the operational strategies for the effective utilization of the generated power will be optimized, aiming to establish both the technical and practical foundations required for commercialization.

REFERENCES

[1] F. Haga, “Current Situation and Challenges in the Utilization of Hot Spring Binary Power Generation” *Journal of Nagano Prefectural University*, Vol. 52, Nos. 3–4, pp. 111–126, 2018.

[2] Ministry of the Environment, “FY2010 Survey on the Introduction Potential of Renewable Energy” pp. 156–159, 2011.

[3] Da Vinci Co., Ltd. Website, *RHE 10kW system*, https://davinci-mode.co.jp/index.php

[4] IHI Corporation Website, *HR series (HR20W)*, https://www.ihi.co.jp/all_news/2013/industrial_general_machine/1190252_1695.html

[5] ADVANCE RIKO, Inc. Website, *ECOR-3-Ft,* https://advance-riko.com/

[6] SankoDenki Co., Ltd. Website, POWER + GENERATOR POWER+4400 https://www.sankoelectric.co.jp/power-generator/

[7] Kobe Steel, Ltd. Website, *MB-70H*, https://www.kobelco.co.jp/releases/2011/1186618_14781.html

[8] Kobe Steel, Ltd. Website, *MB-125S*, https://www.kobelco.co.jp/releases/2013/1188533_13519.html

[9] Daiichi Jitsugyo Co., Ltd. Website, *Thermapower 125MT*, https://www.djk.co.jp/small_binarypower.html

[10] Xenesys Inc. Website, *Mini-DTEC*, http://www.xenesys.com/